*Astronomy & Astrophysics* manuscript no. WASP-39b
February 3, 2011


# WASP-39b: a highly inflated Saturn-mass planet orbiting a late G-type star

F. Faedi[1], S. C. C. Barros[1], D. Anderson[2], D. J. A. Brown[3], A. Collier Cameron[3], D. Pollacco[1], I. Boisse[4,5], G. Hébrard[4,6], M. Lendl[7], T. A. Lister[8], B. Smalley[2], R. A. Street[8], A. H. M. J. Triaud[7], J. Bento[9], O. W. Butters[10], B. Enoch[3], F. Bouchy[4,6], C. A. Haswell[11], C. Hellier[2], F. P. Keenan[1], G. R. M. Miller[3], V. Moulds[1], C. Moutou[12], A. J. Norton[11], D. Queloz[7], A. Santerne[4,6], E. K. Simpson[1], I. Skillen[13], A. M. S. Smith[2], S. Udry[7], C. A. Watson[1], R. G. West[10], and P. J. Wheatley[9]

[1] Astrophysics Research Centre, School of Mathematics and Physics, Queen's University Belfast, University Road, Belfast BT7 1NN. e-mail: f.faedi@qub.ac.uk
[2] Astrophysics Group, Keele University, Staffordshire, ST5 5BG, UK
[3] School of Physics and Astronomy, University of St Andrews, St Andrews, Fife KY16 9SS, UK
[4] Institut d'Astrophysique de Paris, UMR7095 CNRS, Université Pierre & Marie Curie, France
[5] Centro de Astrofísica, Universidade do Porto, Rua das Estrelas, 4150-762 Porto, Portugal
[6] Observatoire de Haute-Provence, CNRS/OAMP, 04870 St Michel l'Observatoire, France
[7] Observatoire astronomique de lUniversité de Genéve, 51 ch. des Maillettes, 1290 Sauverny, Switzerland
[8] Las Cumbres Observatory Global Telescope Network, 6740 Cortona Drive Suite 102, CA 93117, USA
[9] Department of Physics, University of Warwick, Coventry CV4 7AL, UK
[10] Department of Physics and Astronomy, University of Leicester, Leicester, LE1 7RH
[11] Department of Physics and Astronomy, The Open University, Milton Keynes, MK7 6AA, UK
[12] Laboratoire d'Astrophysique de Marseille, 38 rue Frédéric Joliot-Curie, 13388 Marseille cedex 13, France
[13] Isaac Newton Group of Telescopes, Apartado de Correos 321, E-38700 Santa Cruz de Palma, Spain

Received; accepted

**ABSTRACT**

We present the discovery of WASP-39b, a transiting Saturn-mass planet orbiting a late G-type dwarf star with a period of 4.055259±0.000008 d, Transit Epoch $T_0$ = 2455342.9688 ± 0.0002(HJD), of duration 0.1168±0.0008 d. WASP-39b has a mass of 0.28±0.03 $M_J$ and a radius of 1.27±0.04 $R_J$, yielding a mean density of 0.14±0.02 $\rho_J$. Only WASP-17b and WASP-31b have lower densities than WASP-39b, although they are slightly more massive and highly irradiated planets. From our spectral analysis we find WASP-39 to have a metallicity of [Fe/H]= −0.12 dex, which strengthens the observed correlation between planetary density and host star metallicity for the known Saturn-mass transiting planets.

**Key words.** planetary systems – stars: individual: (WASP-39, GSC 04980-00761) – techniques: radial velocity, photometry

## 1. Introduction

The importance of transiting extra-solar planets is related to their geometrical configuration (Sackett 1999). Transit geometry severely constrains the orbital inclination of the planet, allowing accurate measurements of its mass and radius to be derived. The inferred planet's density provides information on the system's bulk physical properties, and thus, is a fundamental parameter to constrain theoretical models of planetary formation, structure and evolution (e.g. Guillot 2005; Fortney et al. 2007; Liu et al. 2008).

To date more than 100 transiting planets have been discovered, which show a huge range of diversity in their physical and dynamical properties. For example, their mass ranges from $\sim 5M_\oplus$ (CoRoT-7 b, Queloz et al. 2009; Pont et al. 2010) to about $12M_J$ (XO-3 b, Johns-Krull et al. 2008; and Hébrard et al. 2008), some planets have radii that agree with models of irradiated planets (Burrows et al. 2007; Fortney et al. 2007), while others are found to be anomalously large (e.g. WASP-12b Hebb et al. 2008 and TrES-4b Southworth 2010, Torres et al. 2008, Mandushev et al. 2007). The diversity in exoplanet densities and hence in their internal compositions is particularly noticed at sub-Jupiter masses. For example, some exoplanets have very high densities and are thought to have a rock/ice cores (e.g. HD 149026b, $\rho_{pl} \simeq 1\rho_J$, Sato et al. 2005), while systems such as TrES-4b ($\rho_{pl} = 0.17\rho_J$, Mandushev et al. 2007), WASP-17b ($\rho_{pl} = 0.06\rho_J$, Anderson et al. 2010a), WASP-31b ($\rho_{pl} = 0.132\rho_J$, Anderson et al. 2010b), and Kepler-7b ($\rho_{pl} = 0.13\rho_J$, Latham et al. 2010) are extreme examples of planets with densities so low that even coreless models have difficulty reproducing their radii (Fortney et al. 2007; Burrows et al. 2007).

Although the majority of the known exoplanets are short-period, Jupiter-mass planets, more recently an increasing number of Saturn-like planets have been discovered (e.g. Enoch et al. 2010), and have encouraged studies of planetary properties and their statistical analysis, searching for possible correlations between planetary parameters (e.g. Enoch et al. 2010; Anderson et al. 2010b; Hartman et al. 2010). To date 27 transiting planets have been discovered with masses in the range $0.15M_J < M_{pl} < 0.6M_J$ [1], similar to Saturn ($M_{saturn} = 0.229M_J$, Standish 1995). The detection and characterisation of signifi-

[1] http://exoplanet.eu/

cantly more bright short-period transiting systems is the key to improve our understanding of planetary structure and evolution.

Here we describe the properties of WASP-39b, a new transiting Saturn-mass planet discovered by the SuperWASP survey. The planet host star WASP-39 belongs to the constellation of Virgo and thus resides in an equatorial region of sky which is monitored by the SuperWASP-North and WASP-South telescopes simultaneously. WASP-39b is the third least dense planet ($\rho_{\rm pl} = 0.14 \pm 0.02\rho_{\rm J}$) discovered from a ground-based transit survey, and belongs to the sample of highly inflated gas giant planets. It provides observational evidence for the mass-radius relation of planetary systems in a poorly sampled region of the parameter space.

We present follow up observations of the new system which establish the planetary nature of the transiting object detected by SuperWASP. We have acquired high precision, high signal-to-noise light-curves using both the Faulkes Telescope North (FTN), and the Euler telescope. We obtained radial velocity measurements using the SOPHIE (1.93–m OHP) and CORALIE (Swiss 1.2–m) spectrographs.

The paper is structured as follows: in § 2 we describe the observations, including the WASP discovery data and the photometric and spectroscopic follow up. In § 3 we present our results for the derived systems parameters, and the stellar and planetary properties. Finally we discuss the implication of the discovery of WASP-39b in § 4.

## 2. Observations

1SWASP J142918.42-032640.1 (2MASS 14291840-0326403), hereafter WASP-39, has been identified in several northern sky catalogues which provide broad-band optical (Zacharias et al. 2005) and infra-red 2MASS magnitudes (Skrutskie et al. 2006) as well as proper motion information. Coordinates and broad-band magnitudes of the star are from the NOMAD catalogue and given in Table 1.

### 2.1. SuperWASP observations

The WASP North and South telescopes are located in La Palma (ING - Canaries Islands) and Sutherland (SAAO - South Africa), respectively. Each telescope consists of 8 Canon 200mm f/1.8 focal lenses coupled to e2v 2048x2048 pixel CCDs, yielding a field of view of 7.8×7.8 square degrees with a pixel scale of 13.7″(Pollacco et al. 2006).

WASP-39 is a $V = 12.11$ star located in an equatorial region of sky monitored by both WASP instruments, significantly increasing the observing coverage on the target. In January 2009 the SuperWASP-N telescope has underwent a system upgrade that improved our control over the main sources of red noise, such as temperature-dependent focus changes (Barros et al. 2011). This upgrade yielded data of unprecedented high quality, and increased the number of planet candidates, flagged in the archive, in particular those with longer period and lower mass (e.g. WASP-38b, Barros et al. 2011; and WASP-39b).

WASP-39 was routinely observed between 2006, July $1^{st}$ to 2010, July $26^{th}$ with a total of 11 WASP fields and 40531 photometric points. Over the 5 WASP seasons only 3 points were taken in 2006 and none during 2007. However, the same field was observed again in 2008, 2009 and 2010 after both WASP telescopes began observing an overlapping equatorial region.

All data were processed with a custom-built reduction pipeline described in Pollacco et al. (2006). The resulting light-curves were analysed using our implementation of the Box Least-Squares and SysRem detrending algorithms (see Collier Cameron et al. 2006; Kovács et al. 2002; Tamuz et al. 2005), to search for signatures of planetary transits. When combined, the SuperWASP light-curves showed a characteristic periodic dip in brightness with a period of $P = 4.055$ days, duration $T_{14} \sim 168$ mins, and a depth $\sim 21$ mmag. Figure 1 shows the discovery photometry of WASP-39b phase folded on the above period, along with the binned phased light-curve. A total of 10 partial or full transits were observed with an improvement in $\chi^2$ of the box-shaped model over the flat light-curve of $\Delta\chi^2 = 825$. We evaluated a signal-to-red noise value of the data following Pont et al. (2006), and determined $S\,N_{red} = 11.65$.

**Table 1.** Photometric properties of WASP-39. The broad band magnitudes are obtained from the NOMAD 1.0 catalogue.

| Parameter | WASP-39 |
|---|---|
| RA(J2000) | 14:29:18.42 |
| Dec(J2000) | -03:26:40.1 |
| B | 12.93±0.25 |
| V | 12.11±0.13 |
| I | 11.34±0.08 |
| J | 10.663±0.024 |
| H | 10.307±0.023 |
| K | 10.202±0.023 |

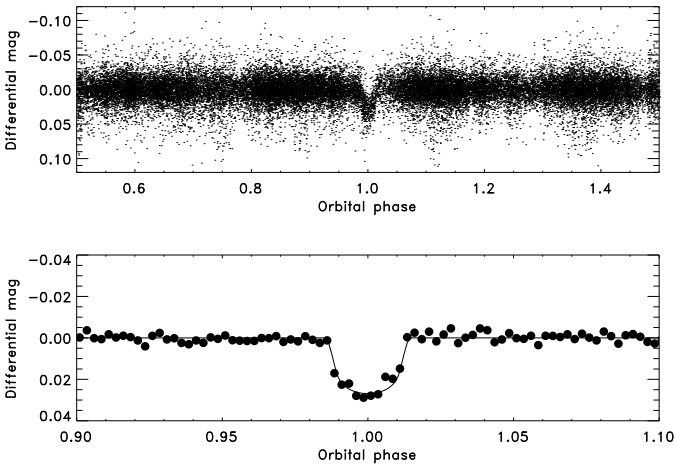


**Fig. 1.** *Upper panel*: Discovery light-curve of WASP-39b phase folded on the ephemeris given in Table 3. *Lower panel*: binned WASP-39b light-curve. Black-solid line, is the best-fit transit model estimated using the formalism from Mandel & Agol (2002).

### 2.2. Spectroscopic follow up

WASP-39 was first observed during our follow up campaign in April 2010 at Observatoire de Haute-Provence (OHP). During our program we have obtained follow up spectroscopy and established the planetary nature of WASP-39b together with three additional systems: WASP-37b (Simpson et al. 2011), WASP-38b (Barros et al. 2011) and WASP-40b (Anderson et al. 2011). Between 2010 April 8 and June 11, we obtained eight radial velocity measurements for WASP-39 using SOPHIE, the fiber-

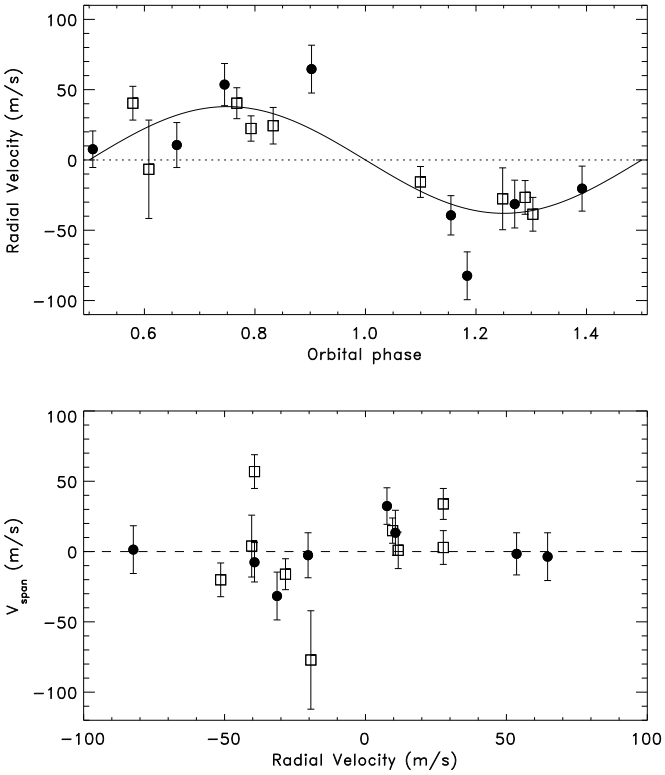


**Fig. 2.** *Upper panel*: Phase folded radial velocity measurements of WASP-39 obtained combining data from SOPHIE (filled-circles) and CORALIE (open-squares) spectrographs. Superimposed is the best-fit model RV curve with parameters from Table 3. The centre-of-mass velocity for each data set was subtracted from the RVs ($\gamma_{\rm SOPHIE}$ = −58.4944 km/s and $\gamma_{\rm CORALIE}$ = −58.4826 km/s). *Lower panel*: we show the bisector span measurements as a function of radial velocity, values are shifted to a zero-mean (< $V_{span}$ >$_{SOPHIE}$= −0.032, < $V_{span}$ >$_{CORALIE}$= −0.051). The bisector span shows no significant variation nor correlation with the RVs, suggesting that the signal is mainly due to Doppler shifts of the stellar lines rather than stellar profile variations due to stellar activity or a blended eclipsing binary.

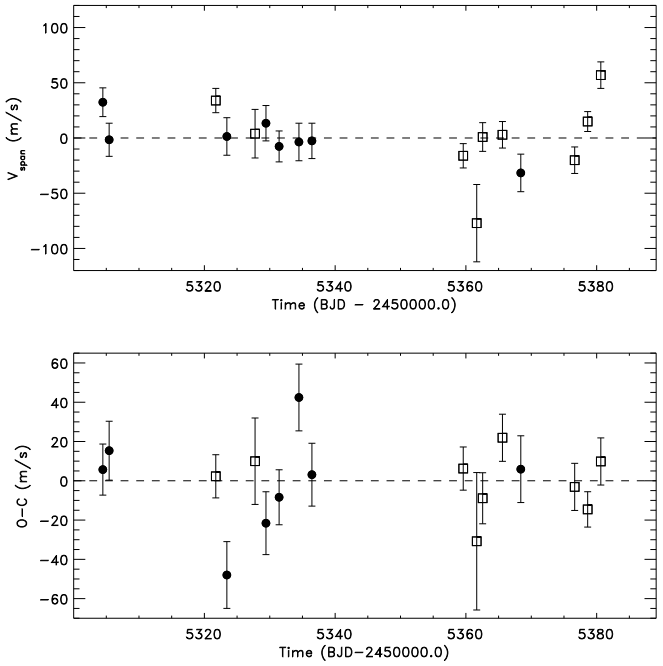


**Fig. 3.** *Upper panel*: The bisector span measurements as a function of time (BJD–2450000.0). *Lower panel*: Residuals from the RV orbital fit plotted against time.

fed echelle spectrograph mounted on the 1.93-m telescope at the OHP (Perruchot et al. 2008; Bouchy et al. 2009). We used SOPHIE in high efficiency mode (R = 40,000) and obtained observations with very similar signal-to-noise ratio (∼30), in order to minimise systematic errors arising from the known Charge Transfer Inefficiency effect of the CCD (Bouchy et al. 2009); although this is now corrected by the data reduction software. Wavelength calibration with a Thorium-Argon lamp were performed every ∼2 hours, allowing the interpolation of the spectral drift of SOPHIE (<3m/s per hour; see Boisse et al. 2010). Two 3″ diameter optical fibres were used, the first centred on the target and the second on the sky to simultaneously measure the background to remove contamination from scattered moonlight. During our observations the contribution from scattered moonlight was negligible as it was well shifted from the target's radial velocity. Nine additional radial velocity measurements were obtained using the CORALIE spectrograph mounted on the 1.2-m Euler Swiss telescope at La Silla, Chile (Baranne et al. 1996; Queloz et al. 2000; Pepe et al. 2002). Observations were obtained during grey/dark time to minimise moonlight contamination. The data were processed with the SOPHIE and CORALIE standard data reduction pipelines, respectively. The radial velocity uncertainties were evaluated including known systematics such as guiding and centring errors (Boisse et al. 2010), and wavelength calibration uncertainties. All spectra were single-lined.

We computed the radial velocities from a weighted cross-correlation of each spectrum with a numerical mask of spectral type G2, as described in Baranne et al. (1996) and Pepe et al. (2002). The cross-correlation with masks of different spectral types (F0, K5 and M5) produced similar radial velocity variation, rejecting a blended eclipsing system of stars with unequal masses as a possible cause of the variation. The radial velocity measurements and line bisector ($V_{span}$) are given in Table 4, and plotted with the best-fit Keplerian model in Figure 2. SOPHIE data are plotted as filled-circles and CORALIE data as open-squares. No significant correlation is observed between the radial velocity and the line bisector suggesting the signal's origin as planetary rather then due to a blended eclipsing binary system, or to stellar activity (see Queloz et al. 2001). We also plot in Figure 3–upper panel, the bisector span measurements as a function of time; and *lower panel*, the residuals from the RV orbital fit against time.

### 2.3. Photometric follow up

In order to allow more accurate light-curve modelling and thus refine the photometric parameters, we obtained two high signal-to-noise transit light-curves of WASP-39b. All photometric data presented here are available from the NStED database [2]. The first full transit was observed with the LCOGT[3] 2m Faulkes Telescope North (FTN) on Haleakala, Maui Hawai'i, on the night of 2010 May 18. The fs03 Spectral Instruments camera was used with a 2×2 binning mode giving a field of view of 10′× 10′ and a pixel scale of 0.303″/pixel. Data were taken through

[2] http://nsted.ipac.caltech.edu

[3] http://lcogt.net

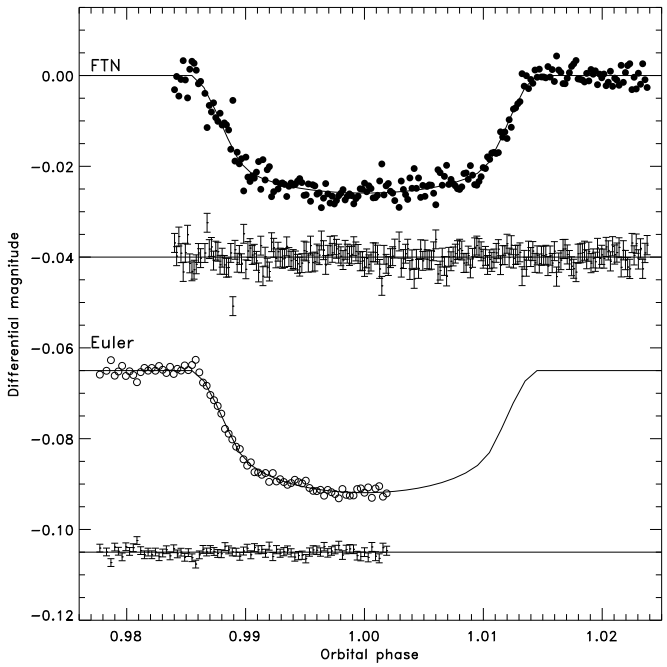


**Fig. 4.** FTN $z-$band and Euler $r-$band follow up high signal-to-noise photometry of WASP-39b during the transit. The Euler light-curve has been ofsetted from zero by an arbitrary amount for clarity. The data are phase-folded on the ephemeris from Table 3. Superposed (black-solid line) is the best-fit transit model estimated using the formalism from Mandel & Agol (2002). Residuals from the fit are displayed underneath.

a Pan-STARRS-z filter and the telescope was defocussed during observations to prevent saturation and allow longer exposure times to be used. The observations were pre-processed using the WASP Pipeline Pollacco et al. (2006) to perform master bias and flat construction, debiassing and flatfielding. Aperture photometry was performed with the the DAOPHOT package (Stetson 1987) within the IRAF[4] environment using a 13 pixel radius aperture. The differential photometry was performed relative to 7 comparison stars that were within the FTN field of view. Additional high signal-to-noise photometry was obtained in the Gunn $r$ filter with the Euler-Swiss telescope on 2010, July 9, only covering a partial transit. Conditions were variable, with seeing ranging from 0.6 ″to 1.7 ″. The Euler telescope employs an absolute tracking system which keeps the star on the same pixel during the observation, by matching the point sources in each image with a catalogue, and adjusting the telescope pointing between exposures to compensate for drifts. The observations were obtained with a slightly defocused (0.1 mm) telescope. All images were corrected for bias and flat field effects and the light-curve was obtained by performing relative aperture photometry of the target and one bright reference star.

Both the FTN and Euler light-curves are shown in Figure 4. The photometry confirms the transit which phases with the ephemeris derived from the WASP discovery photometry.

[4] IRAF is distributed by the National Optical Astronomy Observatory, which is operated by the Association of Universities for Research in Astronomy, Inc., under cooperative agreement with the National Science Foundation.

**Table 2.** Stellar parameters of WASP-39 from Spectroscopic Analysis.

| Parameter | Value |
|---|---|
| $T_{\rm eff}$ | 5400 ± 150 K |
| $\log g$ | 4.4 ± 0.2 |
| $\xi_{\rm t}$ | 0.9 ± 0.2 km s$^{-1}$ |
| $v \sin i^{\star}$ | 1.4 ± 0.6 km s$^{-1}$ |
| [Fe/H] | −0.12 ± 0.10 |
| [Na/H] | −0.04 ± 0.10 |
| [Mg/H] | 0.06 ± 0.11 |
| [Al/H] | 0.01 ± 0.08 |
| [Si/H] | 0.04 ± 0.08 |
| [Ca/H] | 0.01 ± 0.14 |
| [Sc/H] | 0.02 ± 0.19 |
| [Ti/H] | −0.03 ± 0.10 |
| [V/H] | −0.08 ± 0.17 |
| [Cr/H] | −0.07 ± 0.10 |
| [Mn/H] | −0.03 ± 0.20 |
| [Co/H] | −0.10 ± 0.12 |
| [Ni/H] | −0.06 ± 0.09 |
| log A(Li) | < 0.9 |
| Mass | 0.93 ± 0.09 M$_{\odot}$ |
| Radius | 1.00 ± 0.25 R$_{\odot}$ |
| Sp. Type | G8 |
| Distance | 230 ± 80 pc |

**Note:** Mass and Radius estimate using the Torres et al. (2010) calibration. Spectral Type estimated from $T_{\rm eff}$ using the table in Gray (2008).

## 3. Results

### 3.1. Stellar parameters

A total of 9 individual CORALIE spectra of WASP-39 were co-added to produce a single spectrum with a typical S/N of around 50:1. The standard pipeline reduction products were used in the analysis. In order to improve the line profile fitting for equivalent width measurements, the spectrum was smoothed using a Gaussian width $\sigma$ = 0.05 Å. For the $v \sin i^{\star}$ determination the un-smoothed spectrum was used.

Our analysis was performed using the methods given in Gillon et al. (2009). The $H_{\alpha}$ line was used to determine the effective temperature ($T_{\rm eff}$), while the Na I D and Mg I b lines were used as surface gravity ($\log g$) diagnostics. The atmospheric parameters obtained from the analysis are listed in Table 2. The elemental abundances were determined from equivalent width measurements of several clean and unblended lines. A value for microturbulence ($\xi_{\rm t}$) was determined from the Fe I lines using the method of Magain (1984). Quoted error estimates include those given by the uncertainties in $T_{\rm eff}$, $\log g$ and $\xi_{\rm t}$, as well as the scatter due to measurement and atomic data uncertainties.

The projected stellar rotation velocity ($v \sin i^{\star}$) was determined by fitting the profiles of several unblended Fe I lines. A value for macroturbulence ($v_{\rm mac}$) of 2.1 ± 0.3 km s$^{-1}$ was assumed, based on the tabulation by Gray (2008), and an instrumental FWHM of 0.11 ± 0.01 Å, determined from the telluric lines around 6300Å. A best fitting value of $v \sin i^{\star}$ = 1.4 ± 0.6 km s$^{-1}$ was obtained. The stellar mass $M_{\star}$ and radius $R_{\star}$ were estimated using the calibration of Torres et al. (2010).

The non-detection of lithium in the spectrum, the low rotation rate implied by the $v \sin i^{\star}$ and lack of stellar activity (shown by the absence of Ca II H and K emission) all indicate that the star is relatively old. Unfortunately, the gyrochronological age

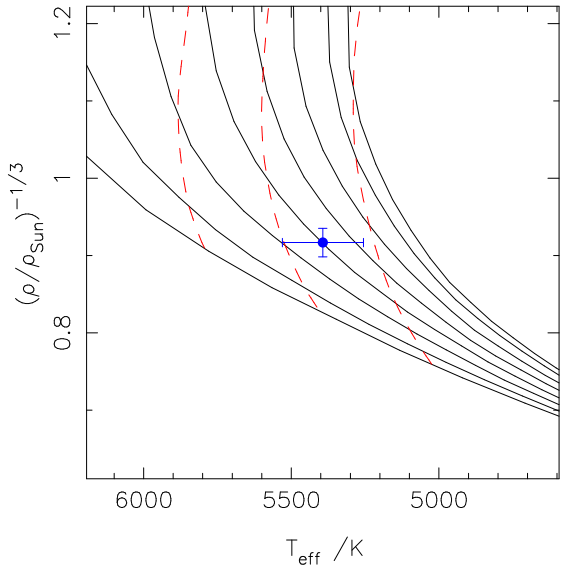


**Fig. 5.** Isochrone tracks from Demarque et al. (2004) for WASP-39 using the best-fit metallicity of [Fe/H]=-0.12 dex and stellar density 1.297 $\rho_\odot$. Solid lines are for isochrones of, let to right: 1.0, 3.0, 6.0, 9.0, 12.0, 15.0, 18.0, and 20.0 Gyr. Dashed lines are for mass tracks of, left to right: 0.8, 0.9, 1.0 $M_\odot$.

estimate from the Barnes (2007) relation ($\sim 5^{+20}_{-4}$ Gyr) can only provide a weak constrain on the age of WASP-39.

The stellar density of $\rho_\star = 1.297^{+0.080}_{-0.074}\,\rho_J$ obtained from the MCMC analysis was used together with the stellar temperature and metallicity values, derived from spectroscopy, in an interpolation of the Yonsei-Yale stellar evolution tracks (Demarque et al. 2004), as shown in Figure 5. Using the best-fit metallicity of [Fe/H]=−0.12 we obtain a mass for WASP-39 of 0.86 ± 0.05 $M_\odot$ and a stellar age of $9^{+3}_{-4}$ Gyr, which is in agreement with the gyrochronological age and it gives a more accurate estimate. The mass obtained from the YY-isochrone fit is somewhat smaller than the value from the Torres et al. (2010) calibration (as it was also found in the analysis of WASP-37 stellar parameters, by Simpson et al. 2011), but their 1-$\sigma$ errors overlap.

### 3.2. Planetary parameters

The planetary properties were determined using a simultaneous Markov-Chain Monte Carlo (MCMC) analysis including the WASP photometry, the follow up FTN and Euler photometry, together with SOPHIE and CORALIE radial velocity measurements. A detailed description of the method is given in Collier Cameron et al. (2007) and Pollacco et al. (2008). The parameters we used in the fit are: the epoch of mid transit $T_0$, the orbital period $P$, the fractional change of flux proportional to the ratio of stellar to planet surface areas $\Delta F = R^2_{\rm pl}/R^2_\star$, the transit duration $T_{14}$, the impact parameter $b$, the radial velocity semi-amplitude $K_1$, the stellar effective temperature $T_{\rm eff}$, metallicity [Fe/H], the Lagrangian elements $\sqrt{e}\cos\omega$ and $\sqrt{e}\sin\omega$ (where $e$ is the eccentricity and $\omega$ the longitude of periastron), and the systematic offset velocity $\gamma$. In this particular case we fitted the 2 systematic velocities $\gamma_{SOPHIE}$ and $\gamma_{CORALIE}$ to allow for instrumental offsets between the two datasets.

Four different sets of solutions were considered: with and without the main-sequence mass-radius constraint in the case of circular orbits and orbits with floating eccentricity. For each solution we have included a linear trend in the systemic velocity, as a free parameter, however we find no significant variation. We used the model of Claret (2000); Claret (2004) for the limb-darkening in the $r$-band, for both WASP and Euler photometry, and in the $z$-band for FTN photometry. Due to the low mass of WASP-39b, the radial velocity data do not offer convincing evidence for an eccentric orbit. We performed a Lucy & Sweeney (Lucy & Sweeney 1971, Eq. 27) F-test, which indicates that there is a 54% probability that the improvement in the fit produced by the best-fitting eccentricity could have arisen by chance if the orbit were truly circular. Moreover, we find that imposing the main-sequence constraint has little effect on the MCMC global solution, thus we decided to adopt no main-sequence prior and circular orbit.

From the above parameters, we calculate the mass $M$, radius $R$, density $\rho$, and surface gravity $\log g$ of the star (which we denote with subscript $\star$) and the planet (which we denote with subscript pl), as well as the equilibrium temperature of the planet assuming it to be a black-body $T_{\rm pl,A=0}$ and that energy is efficiently redistributed from the planet's day-side to its night-side. We also calculate the transit ingress/egress times $T_{12}/T_{34}$, and the orbital semi-major axis $a$. These calculated values and their 1-$\sigma$ uncertainties from our MCMC analysis are presented in Table 3. The corresponding best-fitting transit light curves are shown in Figure 1 and Figure 4, and the best-fitting RV curve in Figure 2.

**Table 3.** System parameters of WASP-39

| Parameter (Unit) | Value |
|---|---|
| $P$ (d) | 4.055259±0.000009 |
| $T_{\rm c}$ (HJD) | 2455342.9688±0.0002 |
| $T_{14}$ (d) | 0.1168±0.0008 |
| $T_{12} = T_{34}$ (d) | 0.0179±0.0009 |
| $\Delta F = R^2_{\rm pl}/R^2_\star$ | $0.0211^{+0.0003}_{-0.0004}$ |
| $b$ | $0.441^{+0.036}_{-0.043}$ |
| $i$ (°) | $87.83^{+0.25}_{-0.22}$ |
| $K_1$ (m s$^{-1}$) | 38±4 |
| $\gamma_{\rm SOPHIE}$ (km s$^{-1}$) | -58.4826±0.0004 |
| $\gamma_{\rm CORALIE}$ (km s$^{-1}$) | -58.4708±0.0004 |
| $e$ | 0 (fixed) |
| $M_\star$ ($M_\odot$) | 0.93±0.03 |
| $R_\star$ ($R_\odot$) | 0.895±0.023 |
| $\log g_\star$ (cgs) | 4.503±0.017 |
| $\rho_\star$ ($\rho_\odot$) | $1.297^{+0.082}_{-0.074}$ |
| $M_{\rm pl}$ ($M_J$) | 0.28±0.03 |
| $R_{\rm pl}$ ($R_J$) | 1.27±0.04 |
| $\log g_{\rm pl}$ (cgs) | $2.610^{+0.047}_{-0.053}$ |
| $\rho_{\rm pl}$ ($\rho_J$) | 0.14±0.02 |
| $a$ (AU) | 0.0486±0.0005 |
| $T_{\rm pl,A=0}$ (K) | $1116^{+33}_{-32}$ |

[a] $T_{14}$: time between $1^{st}$ and $4^{th}$ contact

## 4. Discussion

We report the discovery of a new transiting extra-solar planet, WASP-39b. A simultaneous fit to transit photometry and radial velocity measurements gives a planetary mass of 0.28 ± 0.03 $M_J$ and a radius of 1.27±0.040 $R_J$ which yields a plane-

**Table 4.** Radial velocity (RV) and line bisector span ($V_{\rm span}$ ) measurements of WASP-39.

| BJD−2 400 000 | RV (km s$^{-1}$) | $\sigma_{\rm RV}$ (km s$^{-1}$) | $V_{\rm span}$ (km s$^{-1}$) | Instrument |
|---|---|---|---|---|
| 55321.7484 | -58.455 | 0.011 | -0.017 | CORALIE |
| 55327.7544 | -58.523 | 0.022 | -0.047 | CORALIE |
| 55359.5932 | -58.511 | 0.011 | -0.067 | CORALIE |
| 55361.6552 | -58.502 | 0.035 | -0.128 | CORALIE |
| 55362.5676 | -58.471 | 0.013 | -0.050 | CORALIE |
| 55365.5935 | -58.455 | 0.012 | -0.048 | CORALIE |
| 55376.6394 | -58.534 | 0.012 | -0.071 | CORALIE |
| 55378.6265 | -58.473 | 0.009 | -0.036 | CORALIE |
| 55380.6376 | -58.522 | 0.012 | 0.006 | CORALIE |
| 55304.4704 | -58.475 | 0.013 | 0.000 | SOPHIE |
| 55305.4374 | -58.429 | 0.015 | -0.034 | SOPHIE |
| 55323.4389 | -58.565 | 0.017 | -0.031 | SOPHIE |
| 55329.4184 | -58.472 | 0.016 | -0.019 | SOPHIE |
| 55331.4301 | -58.522 | 0.014 | -0.040 | SOPHIE |
| 55334.4624 | -58.418 | 0.017 | -0.036 | SOPHIE |
| 55336.4477 | -58.503 | 0.016 | -0.035 | SOPHIE |
| 55368.3955 | -58.514 | 0.017 | -0.064 | SOPHIE |

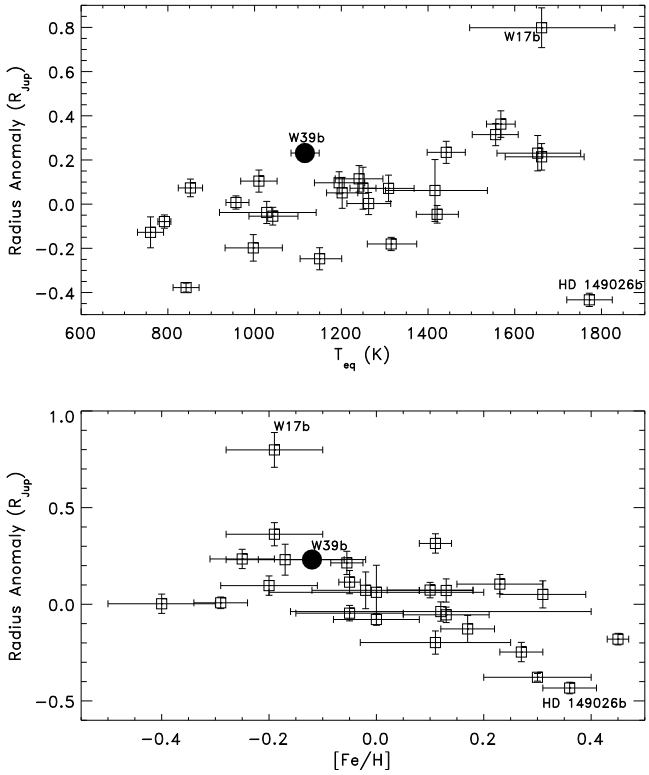


**Fig. 6.** *Upper panel*: The radius anomaly $\mathcal{R} = R_{obs} - R_{pred}$, versus equilibrium temperature for the known Saturn-mass planets from Enoch et al. (2010). *Lower panel*: $\mathcal{R}$ as function of the stellar metallicity [Fe/H] in dex. WASP-39b is indicated with a filled circle.

tary density of 0.141±0.02 $\rho_{\rm J}$. Thus, WASP-39b is the third least dense planet identified by a ground-based transit survey. Only WASP-17b (Anderson et al. 2010a, $\rho_{W17} = 0.06\,\rho_{\rm J}$), and WASP-31b ($\rho_{W31} = 0.132\,\rho_{\rm J}$, Anderson et al. 2010b) have a lower density, however they are slightly more massive planets ($M_{W17}$ = 0.49M$_{\rm J}$ and $M_{W31}$ = 0.48 M$_{\rm J}$), but highly irradiated, with larger and hotter host stars (Anderson et al. 2010a; Anderson et al. 2010b). This implies higher planet equilibrium temperatures for WASP-17b and WASP-31b, compared to WASP-39b. We find WASP-39b to have a highly inflated radius ($R_{pl}$ = 1.265 R$_{\rm J}$), more than 20% larger than the $R_{\rm pl}$ obtained by comparison with the Fortney et al. (2007) and the Baraffe et al. (2008) models for a coreless planet of a similar mass, orbital distance and stellar age. For example, tables presented in Fortney et al. (2007) predict a maximum radius of ∼ 1.05 R$_{\rm J}$ for a 0.24M$_{\rm J}$ planet orbiting at 0.045 AU from a 4.5 Gyr solar-type star. In addition, WASP-39 is smaller, cooler and probably older than the Sun, thus a radius of 1.27 R$_{\rm J}$ is clearly too large for these models. The fact that we do not detect any eccentricity and that the age of the WASP-39b host is >5 Gyr, suggests that it is unlikely that recent tidal circularisation and dissipation could be a cause of the large radius of WASP-39b (Leconte et al. 2010; Hansen 2010). The low metallicity ([Fe/H] = -0.12±0.1) of the WASP-39b host star supports the expected low core-mass of WASP-39b. However, this will only marginally explain the large radius of WASP-39b. Hence, this leads to the hypothesis that some additional physics is at play (Fortney et al. 2009). WASP-39b has a low equilibrium temperature ($T_{\rm pl,A=0}$ = 1116K) and thus appears to belong to the 'pL' class of planets from Fortney et al. (2008). Therefore, an efficient redistribution of heat from the day side to the night side of the planet and no temperature inversion in the atmosphere can be expected.

Of the known transiting systems, WASP-39b joins an increasing number of recently discovered exoplanets with Saturn-like masses. With an increasingly large sample of well-characterised systems, we can begin to make statistical inferences as to the physical reasons behind their diverse nature. Enoch et al. (2010) and Anderson et al. (2011 in prep.), showed that the radii of known low-mass (0.1–0.6 M$_{\rm J}$) planets strongly correlate with equilibrium temperature and host-star metallicity. WASP-39b appears to follow this correlation. Figure 6 shows the *radius anomaly*, $\mathcal{R}$, calculated as in Laughlin et al. (2011), plotted against the planetary equilibrium temperature (upper panel), and as a function of stellar metallicity (lower panel). WASP-39b is indicated with a filled circle. We have plotted the known Saturn-mass planets from Enoch et al. (2010) and added the latest discoveries (for an updated list see the extra-solar planet encyclopedia http://exoplanet.eu/). Laughlin et al. (2011) find that the radius anomaly $\mathcal{R}$ can be attributed to a planetary heating mechanism connected to the planetary magnetic field and core's metallicity, which give rise to Ohmic dissipation, as proposed by Batygin et al. (2011). Batygin et al. (2011) suggests that the extent of this dissipation can explain/maintain the inflated radii of hot Jupiters. The masses of planets in the Saturn-mass range, also appear to correlate with their host star metallicity (Guillot et al. 2006; Burrows et al. 2007), such that low-density planets are found to orbit sub-solar metallicity stars (for example WASP-21 [Fe/H]=−0.4, Bouchy et al. 2010), while higher density planets orbit stars with super-solar metallicity (for example WASP-29 [Fe/H]= 0.11 dex, Hellier et al. 2010, HD 149026 [Fe/H]= 0.36 dex, Sato et al. 2005, and Kepler-9 [Fe/H]= 0.12 dex, Holman et al. 2010). WASP-39 metallicity ([Fe/H]= -0.12 dex) strengthens this correlation (see Figure 6), possibly supporting the core-accretion scenario for planet formation (Guillot et al. 2006; Hartman & others. 2009; Bouchy et al. 2010).

*Acknowledgements.* The SuperWASP Consortium consists of astronomers primarily from Queens University Belfast, St Andrews, Keele, Leicester, The Open University, Isaac Newton Group La Palma and Instituto de Astrofsica de Canarias. The SuperWASP-N camera is hosted by the Issac Newton Group on

La Palma and WASPSouth is hosted by SAAO. We are grateful for their support and assistance. Funding for WASP comes from consortium universities and from the UK's Science and Technology Facilities Council. FPK is grateful to AWE Aldermaston for the award of a William Penney Fellowship. Based on observations made with SOPHIE spectrograph mounted on the 1.9-m telescope at Observatoire de Haute-Provence (CNRS), France and at the ESO La Silla Observatory (Chile) with the CORALIE Echelle spectrograph mounted on the Swiss telescope. The research leading to these results has received funding from the European Community's Seventh Framework Programme (FP7/2007-2013) under grant agreement number RG226604 (OPTICON). FF is grateful to Yilen Goméz Maqueo Chew for proofreading this paper.

## References

Anderson, D. R. et al. 2010a, ApJ, 709, 159
Anderson, D. R. et al. 2010b, ArXiv e-prints
Anderson, D. R. et al. 2011, ArXiv e-prints
Baraffe, I., Chabrier, G., & Barman, T. 2008, A&A, 482, 315
Baranne, A., Queloz, D., Mayor, M., et al. 1996, A&AS, 119, 373
Barnes, S. A. 2007, ApJ, 669, 1167
Barros, S. C. C., Faedi, F., et al. 2011, A&A, 525, A54+
Batygin, K., Stevenson, D. J., & Bodenheimer, P. H. 2011, ArXiv e-prints
Boisse, I. et al. 2010, A&A, 523, A88+
Bouchy, F. et al. 2009, A&A, 505, 853
Bouchy, F. et al. 2010, A&A, 519, A98+
Burrows, A., Hubeny, I., Budaj, J., & Hubbard, W. B. 2007, ApJ, 661, 502
Claret, A. 2000, A&A, 363, 1081
Claret, A. 2004, A&A, 428, 1001
Collier Cameron, A. et al. 2006, MNRAS, 373, 799
Collier Cameron, A. et al. 2007, MNRAS, 380, 1230
Demarque, P., Woo, J., Kim, Y., & Yi, S. K. 2004, ApJ, 155, 667
Enoch, B. et al. 2010, MNRAS, 1531
Fortney, J. J., Baraffe, I., & Militzer, B. 2009, ArXiv e-prints
Fortney, J. J., Lodders, K., Marley, M. S., & Freedman, R. S. 2008, ApJ, 678, 1419
Fortney, J. J., Marley, M. S., & Barnes, J. W. 2007, ApJ, 659, 1661
Gillon, M., Smalley, B., Hebb, L., et al. 2009, A&A, 496, 259
Gray, D. F. 2008, The Observation and Analysis of Stellar Photospheres, ed. Gray, D. F.
Guillot, T. 2005, Annual Review of Earth and Planetary Sciences, 33, 493
Guillot, T., Santos, N. C., Pont, F., et al. 2006, A&A, 453, L21
Hansen, B. M. S. 2010, ApJ, 723, 285
Hartman, J. D. & others. 2009, ApJ, 706, 785
Hartman, J. D. et al. 2010, ArXiv e-prints
Hebb, L. et al. 2008, ArXiv e-prints
Hébrard, G. et al. 2008, A&A, 488, 763
Hellier, C. et al. 2010, ApJ, 723, L60
Holman, M. J. et al. 2010, Science, 330, 51
Johns-Krull, C. M., McCullough, P. R., Burke, C. J., et al. 2008, ApJ, 677, 657
Kovács, G., Zucker, S., & Mazeh, T. 2002, A&A, 391, 369
Latham, D. W. et al. 2010, ApJ, 713, L140
Laughlin, G., Crismani, M., & Adams, F. C. 2011, ArXiv e-prints
Leconte, J., Chabrier, G., Baraffe, I., & Levrard, B. 2010, A&A, 516, A64+
Liu, X., Burrows, A., & Ibgui, L. 2008, ApJ, 687, 1191
Lucy, L. B. & Sweeney, M. A. 1971, AJ, 76, 544
Magain, P. 1984, A&A, 134, 189
Mandel, K. & Agol, E. 2002, ApJ, 580, L171
Mandushev, G., O'Donovan, F. T., Charbonneau, D., et al. 2007, ApJ, 667, L195
Pepe, F., Mayor, M., Galland, F., et al. 2002, A&A, 388, 632
Perruchot, S. et al. 2008, in Society of Photo-Optical Instrumentation Engineers (SPIE) Conference Series, Vol. 7014, Society of Photo-Optical Instrumentation Engineers (SPIE) Conference Series
Pollacco, D. et al. 2008, MNRAS, 385, 1576
Pollacco, D. L. et al. 2006, PASP, 118, 1407
Pont, F., Aigrain, S., & Zucker, S. 2010, ArXiv e-prints
Pont, F., Zucker, S., & Queloz, D. 2006, MNRAS, 373, 231
Queloz, D., Eggenberger, A., Mayor, M., et al. 2000, A&A, 359, L13
Queloz, D., Henry, G. W., Sivan, J. P., et al. 2001, A&A, 379, 279
Queloz, D. et al. 2009, A&A, 506, 303
Sackett, P. D. 1999, in NATO ASIC Proc. 532: Planets Outside the Solar System: Theory and Observations, ed. J.-M. Mariotti & D. Alloin, 189–+
Sato, B. et al. 2005, ApJ, 633, 465
Simpson, E. K., Faedi, F., Barros, S. C. C., et al. 2011, AJ, 141, 8
Skrutskie, M. F. et al. 2006, AJ, 131, 1163
Southworth, J. 2010, MNRAS, 408, 1689
Standish, E. M. 1995, Highlights of Astronomy, 10, 180
Stetson, P. B. 1987, PASP, 99, 191
Tamuz, O., Mazeh, T., & Zucker, S. 2005, MNRAS, 356, 1466
Torres, G., Andersen, J., & Giménez, A. 2010, A&ARv, 18, 67
Torres, G., Winn, J. N., & Holman, M. J. 2008, ApJ, 677, 1324
Zacharias, N., Monet, D. G., Levine, S. E., et al. 2005, VizieR Online Data Catalog, 1297, 0